IEEE Journal of Microwaves

Received 25 August 2023; revised 27 February 2024, 4 April 2024, and 24 April 2024; accepted 26 April 2024. Date of publication 20 May 2024; date of current version 12 July 2024.

Digital Object Identifier 10.1109/JMW.2024.3396353

Dual-Band Reconfigurable Impedance Matching Networks

FARZAD YAZDANI (Member, IEEE) AND MANSOUR R. RAAFAT (Life Fellow, IEEE)

(Regular Paper)

[1]Department of Electrical and Computer Engineering, University of Waterloo, Waterloo, ON N2L 3G1, Canada

CORRESPONDING AUTHOR: Farzad Yazdani (e-mail: yazdani@ieee.org).

ABSTRACT This article presents a novel methodology for designing Dual-band Reconfigurable Impedance Matching Networks (Db-RIMNs) using a cascade network of tunable filters and phase shifters. The proposed design can be used to match frequency dependent and impedance variable dual-band loads. The theory of operation, the design considerations, and the design procedure are provided. Moreover, a prototype circuit is designed for a dual-band variable load at sub-6 GHz bands. The performance of the proposed design is not restricted by the range of realizable characteristic impedances. Moreover, the achievable impedance coverage and frequency ratio of the two bands are not restricted by the circuit fabrication limitations. Finally, the performance in terms of matched bandwidth and losses are investigated. The simulation and measurement results for a fabricated prototype are in close agreement. The proposed design has a wide range of anticipated applications in design of concurrent dual band power amplifiers, multiband antennas, phased arrays, to name a few. The cascade architecture of tunable filters and phase shifters is the sole published design for Db-RIMNs in the literature.

INDEX TERMS Reconfigurable, tunable, dual-band, impedance matching network, concurrent matching, 5G.

I. INTRODUCTION

NOVEL communication systems, including 5G cellular networks and software defined/cognitive radio technologies, call for compact, multi-band, and reconfigurable circuit components. Specifically, multi-band Power Amplifiers (PAs) and multiband antennas are widely employed in 5G systems. Simultaneously, these devices need to be tunable to cover numerous bands. Impedance tuners are fundamental microwave components that allow maximum power transfer between different components. An increasing number of multiband components such as antennas, PAs, power dividers, and baluns, among others are being introduced, which require multiband matching networks. As a result, the desired matching networks should be able to simultaneously address the variable frequency bands (shift in frequency) and variable impedance of the different components [1], [2]. In more detail, the requirements for the multiband impedance tuners include varying frequency ratios, wide impedance coverage at each frequency, low loss, and high power performance. Moreover, it is desirable for the design of tuners for each band to be independent from the other bands.

A handful of literature present dual band matching networks using multi-section transmission line circuits. For example, a parallel and series stub solution is presented in [3], and a three section series transmission line segment solution is presented in [4]. However, these solutions are suitable for fixed load impedances and they cannot be used as tunable solutions because they rely on the characteristic impedance of transmission lines, which cannot be conveniently tuned. Moreover, there is a limited range of transmission line characteristic impedance that can be practically realized. This limitation limits the range of load impedances that can be matched using such solutions.

A handful of works use switches to select the matching frequencies. In [5], a front-end architecture is proposed, which is composed of two tunable single band impedance tuners. A pair of switches select either of the impedance tuners and thus the operation band. In [6], semiconductor switches are used on

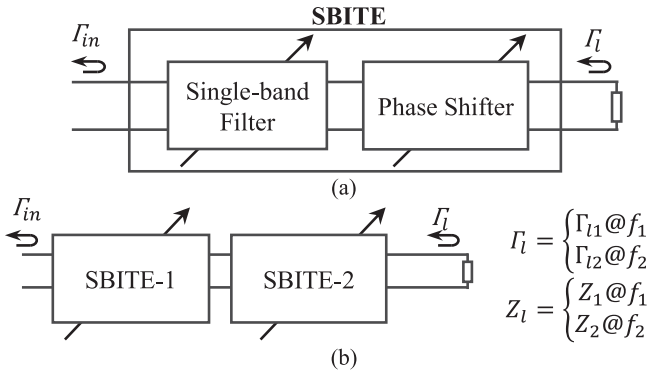

FIGURE 1. Proposed circuit architectures for the DB-RIMNs, (a) a SBITE and (b) cascade architecture.

Transmission Line Transformers (TLTs) to achieve matching at different frequencies. In [7], a T-network matching network is loaded by two switched capacitors to provide matching at 2.4 GHz or 5 GHz. However, these solutions operate at a single frequency at a time and cannot provide simultaneous matching at different bands.

A novel design methodology for matching networks is presented in [8] based on High-Pass Filters (HPFs) and Low-Pass Filters (LPFs) transmission line phase shifters. Although this method is employed for matching a constant load impedance, its independence to the characteristic impedance makes it a suitable candidate for designing tunable matching networks.

This paper proposes a novel category of Dual-band Reconfigurable Impedance Matching Networks (Db-RIMNs), which employ tunable filters and phase shifters. The proposed Db-RIMNs are capable of providing matching between dual band loads with variable impedances and frequency ratios. The proposed approach decouples the impedance coverage from the characteristic impedance of transmission lines, which leads to a wide range of impedance coverage in each band. Moreover, the proposed methodology can be applied to multiband applications. The proposed Db-RIMN concept is in general applicable to high power applications. However, the linearity and operating input power limitations are mainly determined by the power handling capability of the tuning elements used.

The structure of the paper is as follows. First, the tunability of dual-band matching networks is discussed by setting the requirements for employing the concept of tunable filters and phase shifters in designing Db-RIMNs. Accordingly, the design procedure and arguments regarding the different combinations of filters, tuning elements and phase shifters are presented. The remainder deals with a design example and measurements in the sub-6 GHz region, where the center frequency of the two bands can vary in addition to load variation at each band. The design example is presented for a frequency ratio as low as 1.09. Bands with such low frequency ratios cannot be matched using current fixed dual-band matching networks due to the TL impedance constrains [4]. The design example is intended to operate at sub-6 GHz region for 5G networks. Moreover, the frequencies of 3.4 GHz and 3.7 GHz are chosen as an extreme case in terms of the performance of the tuning elements. The design example is provided as a proof of concept, but the proposed method can be employed for loads with larger frequency ratios, wider bandwidths, and at different frequencies.

II. ANALYSES OF PROPOSED CONCEPT

A. NETWORK ARCHITECTURES

The proposed concept is intended to provide matching at the two frequencies independent from each other. This is accomplished by employing two Single Band Impedance Tuning Elements (SBITEs). Each SBITE provides impedance tuning at one of the bands, but has a limited impact on the matching of the other band. A SBITE can be realized by a cascade combination of a microwave filter and phase shifter as shown in Fig. 1(a), where arrows denote the tunability of these components. For an arbitrary SBITE terminated in a load with a reflection coefficient Γ_l, the input reflection coefficient can be written as

$$\Gamma_{in}^{SBITE} = S_{11}^{SBITE} + \frac{S_{12}^{SBITE} S_{21}^{SBITE} \Gamma_l}{1 - S_{22}^{SBITE} \Gamma_l}. \tag{1}$$

Using unitary conditions for lossless and reciprocal networks, it can be shown that

$$\Gamma_{in}^{SBITE} = 0, \text{ if } S_{22}^{SBITE} = \Gamma_l^*, \text{ and} \tag{2}$$

$$\Gamma_{in}^{SBITE} = |\Gamma_l| \left(\angle\Gamma_l + 2\angle S_{12}^{SBITE}\right), \text{ if } S_{11}^{SBITE} = S_{22}^{SBITE} = 0. \tag{3}$$

Equation (2) refers to a condition where the SBITE is complex conjugate matched to Γ_l at its output, which in return leads to no power reflected back from its input port. A SBITE in this state is called a "matching" SBITE. On the other hand, (3) refers to a condition where the SBITE is matched to Z_0. In this case, the input reflection coefficient has the same magnitude as the termination load, but with a modified phase. A SBITE in this state is called a "passing" SBITE.

This work builds on the method presented in [8] for fixed dual-band loads, and makes a case for designing Db-RIMNs for impedance and frequency variable loads. The circuit architecture of the proposed Db-RIMN is illustrated in Fig. 1(b). It is composed of two SBITEs connected in cascade configuration. The termination is a dual-band variable load defined by reflection coefficients Γ_{l1} and Γ_{l2} at two frequencies f_1 and f_2, respectively. Note that any of the reflection coefficients and frequencies can be variable. For the reference $f_1 < f_2$. Each SBITE is tuned to operate as a matching SBITE at one of the bands, and as a passing SBITE at the other. Moreover, the two SBITEs should have opposite states at each band, i.e., one is passing while the other is matching and vice versa.

As illustrated in Fig. 2, the circuit performance can be demonstrated by plotting the reflection coefficient after each block looking toward the load. At f_1, the SBITE-1 and SBITE-2 are in matching and passing states, respectively. At f_2, their states are swapped. To satisfy (2) and (3), the phase shifters need to pass the signal at both bands. This can

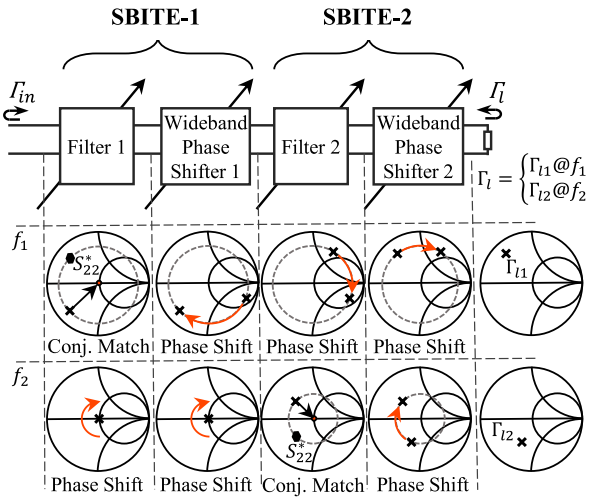

FIGURE 2. Block diagram of the proposed Db-RIMN and its step-by-step performance breakdown, adapted from.

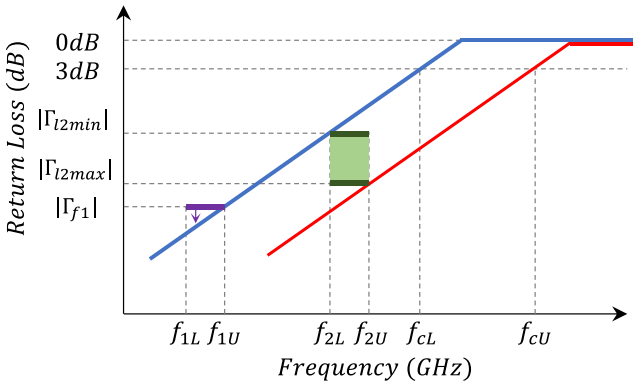

FIGURE 3. Filter requirements for a tunable LPF to provide matching at the higher band.

be achieved using wideband phase shifters or dual-band phase shifters. Moreover, Filter 1 and Filter 2 must have transition band at f_1 and f_2, with output reflection coefficients with the same magnitudes as Γ_{l1} and Γ_{l2}, respectively. In addition, the Filter 1 and Filter 2 must have passbands over f_2 and f_1, respectively. Accordingly, the matching conditions can be written as [8]:

$$\left|S_{22}^{Filter-1}(f_1)\right| \angle(2\angle S_{21}^{Filter-2}(f_1) + 2\varphi_2(f_1) + \angle S_{22}^{Filter-1}(f_1) + 2\varphi_1(f_1)) = \Gamma_{l1}^*, \text{ and} \quad (4)$$

$$\left|S_{22}^{Filter-2}(f_2)\right| \angle\left(\angle S_{22}^{Filter-2}(f_2) + 2\varphi_2(f_2)\right) = \Gamma_{l2}^*, \quad (5)$$

where, φ_1 and φ_2 represent the phase shifts of phase shifters 1 and 2, respectively. Therefore, the following conditions need to be met for the cascade architecture to be operable:

1) The filters used in the passing SBITEs shall have a passband over the transition band of the filters used in the matching SBITEs.
2) The phase-shifters shall provide a maximum of 180° of phase shift at their respective frequencies.
3) The phase-shifters shall be operable at both frequency bands. This can be achieved by wideband or dual-band phase shifters.
4) The tuning of the matching SBITE shall not result in significant degradation in the return loss of the passing SBITE.

Although, we are presenting these conditions for the dual-band case, they can be also used for multi-band designs. For example, the first condition in a tri-band case would require RIMN to use a tunable LPF responsible for matching at the highest band, a tunable HPF for matching at the lowest band, and a Band-Stop Filter (BSF) for the middle band. Each filter must have passband over the two other bands. The three other conditions remain the same as long as the phase shifters cover the three bands.

As a proof of the concept, a Db-RIMN will be designed in the reminder of this paper. In the following, the design considerations for tunable filters are studied in more detail, which will be followed by a design example.

B. FILTER REQUIREMENTS

Fig. 3 illustrates the return loss of a hypothetical LPF. This filter is used as Filter-2 in SBITE-2 that has a passing state over a lower band between f_{1L} and f_{1U}. The SBITE-2 also has a matching state over a higher band between f_{2L} and f_{2U}. The reflection coefficient of the load varies between $\Gamma_{l2\text{min}}$ and $\Gamma_{l2\text{max}}$ over the higher band. The return loss is also intended to be better than Γ_{f1} over the lower band to ensure the passing state for SBITE-2 over the lower band. The return loss is depicted when the filter is tuned to have a cutoff frequency shift between f_{cL} and f_{cU}, without changing the order or type. This shift in cutoff frequency allows the return loss magnitude to cover the values between $|\Gamma_{l2\text{min}}|$ and $|\Gamma_{l2\text{max}}|$ over the higher band, while the SBITE-2 maintains a passing state over the lower band. This figure can be used to determine the order of the filter and its tuning range.

The order of the filter can be determined using the slope of the return loss over the transition band. The goal is to determine the lowest order of the LPF with a return loss equal to $|\Gamma_{f1}|$ and $|\Gamma_{l2\text{min}}|$ at f_{1U} and f_{2L}, respectively. Increasing the order of the LPF beyond this minimum value would result in a better performance at f_{1U}, but also in excessive circuit complexity. Note that the slope of return loss is in inverse relation with the frequency ratio f_{1U}/f_{2L}. Moreover, the roll-off slope is directly proportionate to the ratio of $|\Gamma_{l2\text{min}}|$ and $|\Gamma_{f1}|$.

The reflection coefficient of a filter is associated with its power loss ratio, P_{LR}, through [9]

$$|\Gamma|^2 = \frac{P_{LR} - 1}{P_{LR}}. \quad (6)$$

As given in the Appendix, one can derive the minimum order for a maximally flat LPF with 3dB insertion loss at f_{cL},

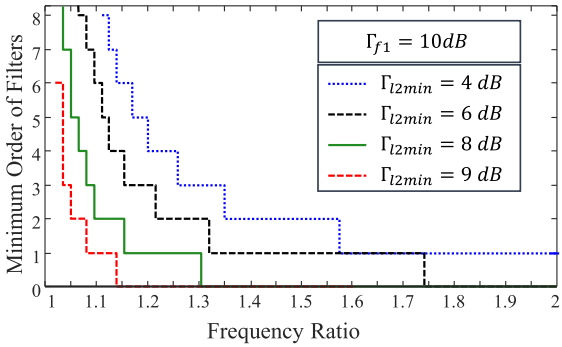

FIGURE 4. Minimum required order of a maximally flat LPF.

as

$$N = \frac{\log\left(\frac{1-|\Gamma_{f1}|^2}{1-|\Gamma_{l2\min}|^2}\right)}{2} + \log\left(\frac{|\Gamma_{l2\min}|}{|\Gamma_{f1}|}\right) \Big/ \log\left(\frac{f_{2L}}{f_{1U}}\right). \tag{7}$$

Fig. 4 depicts the minimum order of a maximally flat LPF. Note that since the filter order is an integer, the graph takes a staircase form. The minimum filter values can be plotted versus the frequency ratio f_{1U}/f_{2L}, for a given value for $|\Gamma_{f1}|$ and a few values for $|\Gamma_{l2\min}|$. For instance, Fig. 4 is plotted for $|\Gamma_{f1}| = 10\ dB$ and $|\Gamma_{l2\min}|$ between 4 dB and 9dB. Note that the return loss is steepest over the transition band for $|\Gamma_{l2\min}| = 4\ dB$ and flattest for $|\Gamma_{l2\min}| = 9\ dB$. Hence, a higher order LPF is needed for $|\Gamma_{l2\min}| = 4\ dB$ compared to the other values and for a given frequency ratio. Moreover, the minimum order of the filter dramatically increases for small frequency ratios. As given in the Appendix, similar expressions can be derived for HPF filters used as Filter 1 in the SBITE-1 by substituting the frequencies and reflection coefficients. The expressions for other types of filters (e.g., Chebyshev filters) can be derived using a similar process.

To determine the tuning range for the filter, one can write

$$\log\left(\frac{f_{cL}}{f_{cU}}\right) = \log\left(\frac{f_{2L}}{f_{2U}}\right) + \frac{\log\left(\frac{|\Gamma_{l2\max}|}{|\Gamma_{l2\min}|}\right)}{N} + \frac{\log\left(\frac{1-|\Gamma_{l2\min}|^2}{1-|\Gamma_{l2\max}|^2}\right)}{2N}. \tag{8}$$

Equations (7) and (8) provide theoretical support for the proposed design method. However, for a tunable filter the passband ripple and roll-off rate would change from state to state. This is because continuous tuning is done only using tunable capacitors. Therefore, the analytical expressions can only serve as a rough estimate and the filter design would require further optimization based on the tuning elements used.

The filters should have steep roll-off while maintaining low-loss and low-ripple passband. This can be realized by a pair of HPF and LPFs. However, the order of these filters need to increase as the frequency ratio between the two bands decreases. Moreover, employing tunable HPF filters adds another challenge associated with the use of series variable capacitors [8]. Alternatively, BPF filters can be used by tuning their center frequencies. This is specifically convenient for wideband BPFs (as presented in [10]). Tuning of the center frequency can be achieved by applying a single bias voltage to identical tuning elements attached to the end of open circuited stubs.

C. DESIGN PROCEDURE

This section provides a brief description of the design steps for Db-RIMNs. Note that these steps can be generalized for multi-band RIMNs as well. The design steps as follows:

1) Characterize the dual-band load. Depending on the application, the load impedance can vary over frequency and time. Determine the reflection coefficient range at the two bands. The required coverage may occupy specific region of the Smith chart (e.g., for optimum impedance matching of a dual-band power amplifier), or cover a ring around the center of the Smith chart (e.g., for tunable antenna matching).
2) Characterize the tuning elements: This includes the tuning range and quality factor range
3) Design the tunable filters: Determine the type and lowest order for the filters based on the frequency ratio and the reflection coefficients range of the load for each band. Design Filter 1 and Filter 2 considering the tuning range of the tuning elements. Assess whether tuning the filters can cover the magnitude range of the load. If coverage is inadequate, repeat this step to select a different filter type and order. Optimize the model further to achieve desired coverage.
4) Design the tunable phase shifters: Determine the type of the phase shifters (i.e., wideband, multiband, direct, or reflection type) based on the frequency ratio and the phase range of the load at each frequency. Assess whether phase shifters can provide the phase shift range of the load.
5) Design Verification: A full-wave simulation of the circuit is necessary to account for the coupling between filters and phase shifters.

III. CIRCUIT DESIGN

In this section, the performance of the proposed Db-RIMN is demonstrated through a design example. The two bands are at a vicinity of 3.4 GHz and 3.7 GHz. A matched bandwidth of at least 50 MHz at each band was targeted to resemble sub-6 GHz 5G applications. The load is assumed an antenna that is required to operate over two bands. The antenna impedance varies with frequency over each band with a reflection coefficient between 5dB and 10dB and with any phase value. It should be noted that the BST tuning elements used are not capable to handle high power levels. Therefore, the design example discussed in this paper is intended for low-power applications.

For tuning elements, Packaged Barium Strontium Titanate (BST) tunable capacitors are considered because of their relatively higher quality factors compared to semiconductor varactors. The used tuning elements have a capacitance ratio

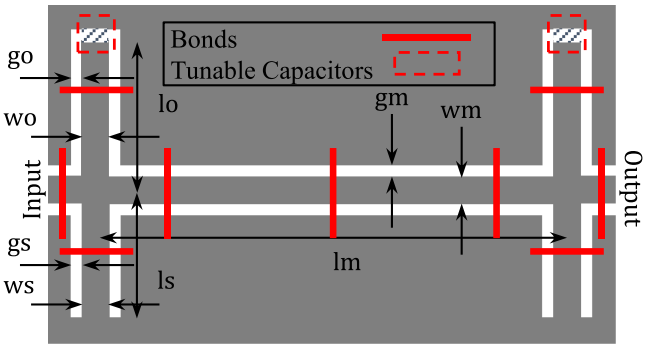

FIGURE 5. Parametric layout of the tapped BPFs using CPW segments and tunable capacitors.

of 4.65. The average quality factor is 30 from experimental characterization of the BST varactors. Only one bias voltage is intended for each of the filters and phase shifters to simplify the tuning process. Accordingly, the Db-RIMN circuit sub-components are developed based on Rogers RO3010 substrates with dielectric constant of 10, thickness of 25 mil, loss tangent of 0.0022, and 17 μm copper metal layers. Note that the implementation technique, including the limited quality factor of the tuning elements and wirebond, may impose limitations in terms of matched bandwidth and insertion loss.

A. TUNABLE BPFS

The schematic of the tunable filters and their dimensions are depicted in Fig. 5. The filter is composed of two resonators that are coupled to each other using a 90° transmission line segment. Each resonator is composed of a short circuited and an open circuited stubs, which together form a parallel LC resonator.

The open-ended segments for the two resonators are terminated by identical tunable BST capacitors. The filters are implemented using CPW lines and the ground planes are connected using wirebonds.

The filters are synthesized initially without the tunable capacitors. Consequently, a full-wave HFSS model is developed where tunable capacitors are replaced by matched ports. Then, the simulated S-parameters of the model are exported to Keysight ADS, where the capacitor ports are terminated with tunable capacitors. The TL segments are optimized to mimic the behavior of the initial synthesized model and improve the insertion loss. The BSTs used for tuning Filter 1 and Filter 2 have the maximum value of 3 pF and 1 pF, respectively. Note that the entire tuning range of the capacitors are not needed. Filter 1 and the Filter 2 only need values between 0.8 pF and 1.6 pF, and 0.2 pF and 0.5 pF, respectively. The simulation results for the designed filters are plotted in Fig. 6. Fig. 6(a) shows the return losses of the Filter 1 loaded by a 3 pF capacitor (i.e., maximum value of the BST), and Filter 2 when it is loaded by a 0.05 pF capacitor (i.e., miniscule value of the BST). Note that the return loss of Filter 1 shifts to higher frequencies by reducing the value of the BST. In contrast, the Filter 2 response shifts to lower frequencies by

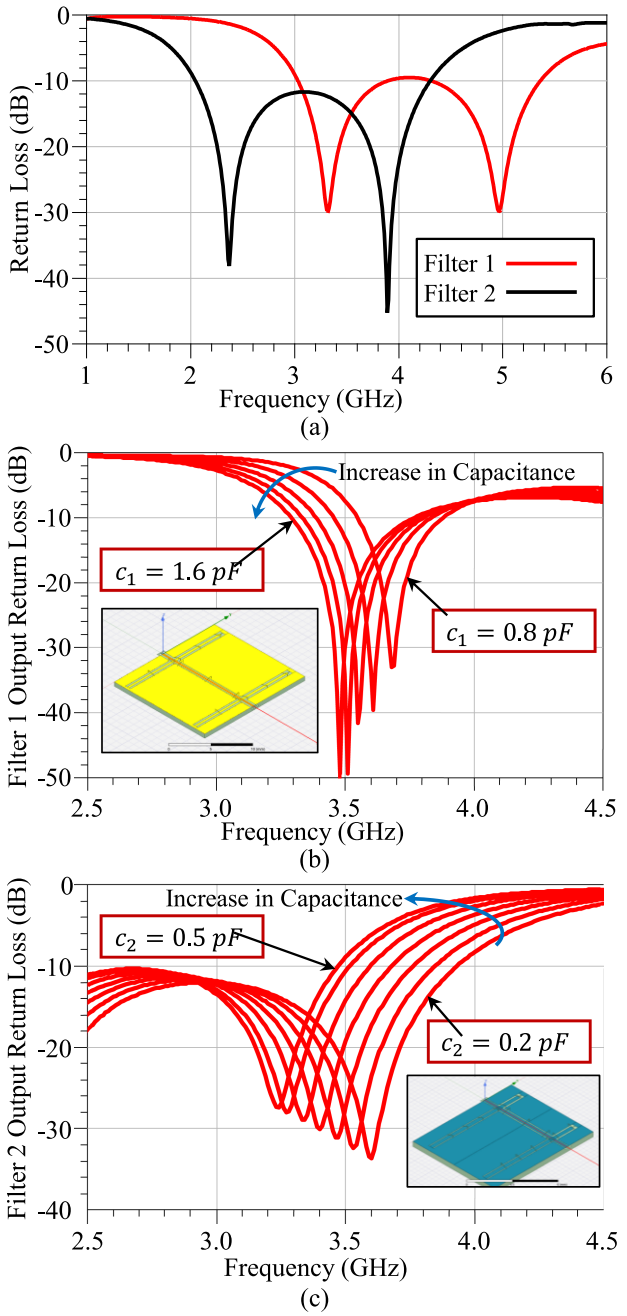

FIGURE 6. Simulated return loss of the filters, (a) filter responses without tuning, (b) filter-1 loaded by c_1 with values ranging from 0.8 pF to 1.6 pF, (c) filter-2 loaded by c_2 with values ranging from 0.2 pF to 0.5 pF.

increasing the value of the BST capacitor. Fig. 6(b) shows the return loss response of Filter 1 for the BST values between 0.8 pF and 1.6 pF. As can be seen, the return loss of Filter 1 covers reflection coefficients of better than 4 dB at 3.4 GHz, while maintaining a passband with better than 12 dB return loss at 3.7 GHz. Similarly, Fig. 6(c) shows the response of Filter 2 for the BST values between 0.2 pF and 0.5 pF. Filter 2 has a return loss of better than 15 dB around 3.4 GHz, while covering reflection coefficients of better than 3 dB at 3.7 GHz.

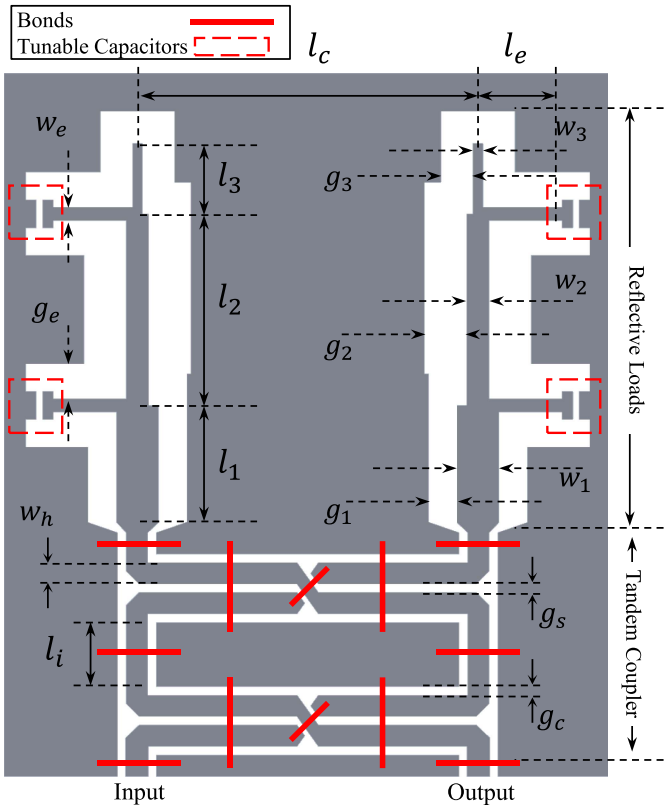

FIGURE 7. Schematic of the proposed RTPS. Dimensions in μm: $l_c = 7977, l_e = 3973, l_1 = 7747, l_2 = 7500, l_3 = 1650, l_i = 1500, g_1 = 670, g_2 = 1000, g_3 = 755, g_c = 206, g_s = 200, g_e = 823, w_1 = 980, w_2 = 523, w_3 = 230, w_h = 500$,w_e=311 .

B. WIDEBAND TUNABLE PHASE SHIFTER

Current state of the art reconfigurable phase shifter designs fall short of meeting the requirements presented in the beginning of this section for the following reasons. Firstly, non-tunable designs [11], [12] and switched designs [13], are not able to provide high-resolution phase shift. Secondly, their loss often increases when their number of states increases. Thirdly, MMIC solutions [14] have limited quality factor and their implementation in lower frequencies becomes large and lossy.

Reflection Type Phase Shifters (RTPSs) are employed because of their compact size compared to direct phase shifters (e.g., loaded line). Moreover, they use fewer tuning elements. A tunable RTPS is composed of two tunable reflective loads connected to the coupled and through ports of a quadrature hybrid coupler. The phase shifters are intended to provide at least 180° of continuous phase shift to address (4) and (5). A schematic of the proposed RTPS and its dimensions are depicted in Fig. 7. As stated in [15], [16], and [17], the range of phase shift achieved using single tuning element reflective loads for RTPSs is less than 180°. Accordingly, a 2-element reflective load is used. It is designed using GCPW lines to avoid further wirebonds. Each reflective load is composed of a three TL segment main branch and two extension stubs, which are terminated in the variable capacitors. The extensions stubs are connected to the main branch using T-junctions. Tandem couplers are used because they require less fabrication tolerance compared to traditional designs, which allows PCB fabrication of the proposed circuit. In addition, tandem couplers have wider bandwidths compared to branch-line couplers [18].

The BST used for the proposed RTPS have a maximum capacitance of 1.5 pF with an average quality factor of about 30. The circuit shown in Fig. 8 is optimized in HFSS. The extracted S-parameters are then terminated in measured BST values. The simulation results are shown in Fig. 8. As can be seen, a phase shift of at least 200° is achieved by modifying the capacitor value from 0.32 pF to 1.5 pF. The insertion and return losses are better than 1.75 dB and 14 dB throughout the frequency range of 3 GHz - 4 GHz. Fig. 9 investigates the impact of the capacitor imperfection on the insertion loss of the proposed RTPS. As can be seen, using a tuning element with a higher Q values can considerably reduce the insertion loss of the phase shifter.

C. DUAL-BAND IMPEDANCE COVERAGE

The final layout of the proposed Db-RIMN is presented in Fig. 10. One way to demonstrate the dual-band impedance coverage is by demonstrating the independent coverage at each band. First, the circuit is simulated using a broadband 50 Ω load and the tuning capacitors are tuned to achieve matching at both frequencies. Then the coverage at each band is demonstrated by tuning the SBITE-1 and SBITE-2 separately. Fig. 11(a) shows the coverage achieved by tuning only the SBITE-2. As can be seen, the output reflection coefficients remain inside the 10 dB circle at 3.4 GHz, while coverage is demonstrated for the area within the 5 dB circle at 3.7 GHz. In addition, Fig. 11(b) shows the coverage achieved by tuning only the SBITE-1. Consistent coverage for the impedances within the 5 dB circle at 3.4 GHz is shown in this figure as well. Fig. 11(a) and (b) together show that in the majority of cases, the two bands can be matched with limited impact on each other.

Fig. 12 plots the return loss over frequency for a selection of states. For Fig. 12(a), the SBITE-1 is in passing state and SBITE-2 is matching. As can be seen, the output return loss remains better than 12 dB at 3.4 GHz. The results at 3.7 GH, illustrates that loads with reflection coefficient between 5 dB and 15 dB can be matched. Note that the return loss remains better than 10 dB from 3.27 GHz to 3.5 GHz. Therefore, this band can be used as the lower band of the proposed Db-RIMN. Similarly, Fig. 12(b) is plotted by keeping the SBITE-2 in a passing state and tuning the SBITE-1. Here, the output return loss remains better than 15 dB at 3.7 GHz. The results shown at 3.4 GHz illustrates that loads with reflection coefficient better than 5 dB can be matched. Likewise, the return loss remains better than 10 dB between 3.62 GHz and 3.96 GHz. However, the quality factor of the BSTs degrade dramatically beyond 3.8 GHz. Therefore, a higher band of between 3.6 GHz to 3.8 GHz can be used by the proposed Db-RIMN.

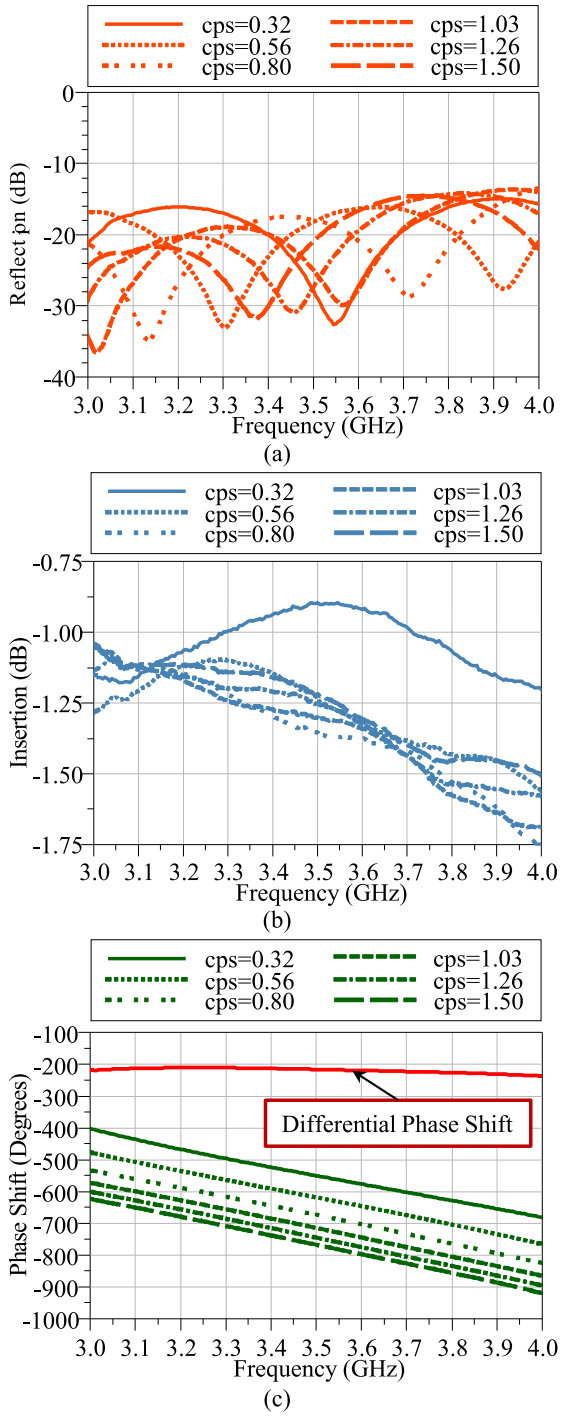

FIGURE 8. Simulated results for the RTPS sub-component when loaded by cps with values ranging from 0.32 pF to 1.5 pF (a) return loss, (b) insertion loss, and (c) phase shift.

IV. MEASUREMENT RESULTS

Prototypes of the proposed Db-RIMN are fabricated on RO3010 substrates. The Gold Immersion surface finish is used to allow wirebonding as well as attachment of the BSTs. Fig. 13 shows the photos of the fabricated and assembled circuits. The size of the entire circuit, excluding SMA connectors and headers, is 45 mm by 77 mm. The diced filters

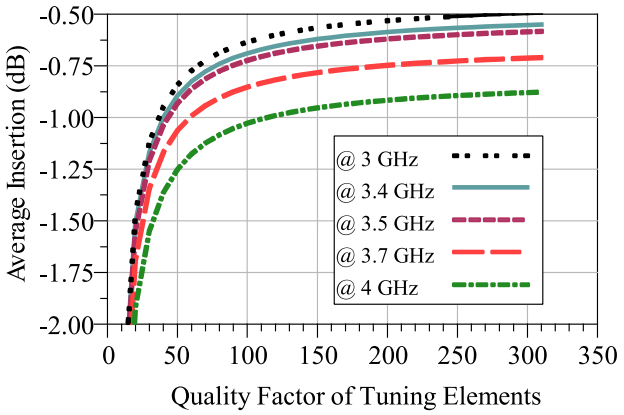

FIGURE 9. Simulated average insertion loss for the RTPS sub-component based on the quality factor of BST tunable capacitor.

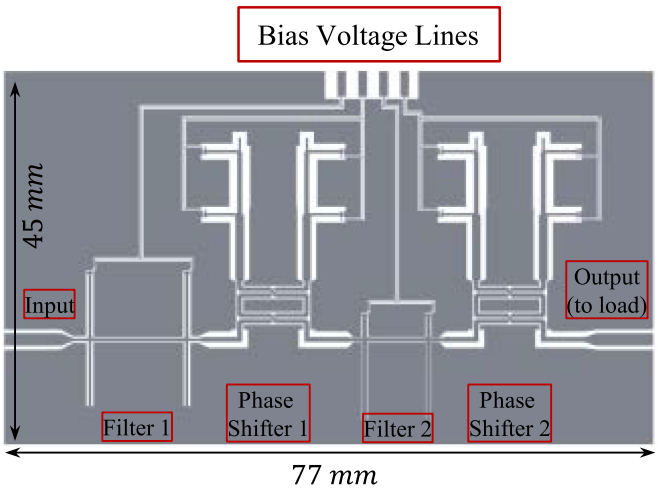

FIGURE 10. Scaled layout of the proposed Db-RIMN, where sub-components are highlighted. SBITE-1 is composed of Filter-1 and Phase Shifter 1, and SBITE-2 is composed of Filter-2 and Phase Shifter 2.

and phase shifters are measured separately for verification and loss measurements. The measurements are performed using Keysight PNA Network Analyzer model N5227B.

A bias voltage of between 2 V and 17 V are applied to the phase shifter and the measurement results are plotted in Fig. 14. The measurement results presented in Fig. 14 agree well with the simulation results presented in Fig. 8. The variation in insertion loss is due to the variation in quality factor of the BSTs. Note that higher bias voltages lead to smaller capacitor values and higher quality factor than the assumed 30. Moreover, the 2 V bias is associated to larger than 1.5 pF. This leads to a significantly small quality factor and an insertion loss of more than 1 dB. Since the achieved phase shift is more than 220°, the lossy states are not needed. The measurement results for the filters are shown in Fig. 15. Here the bias for Filter 1 varies between 4 V and 10 V. For Filter 2, it varies between 10 V and 17 V. As can be see, each filter degrades the insertion loss by at least 1 dB over their passbands, which is mainly due to the addition of the wirebonds and limited quality factor of the BSTs.

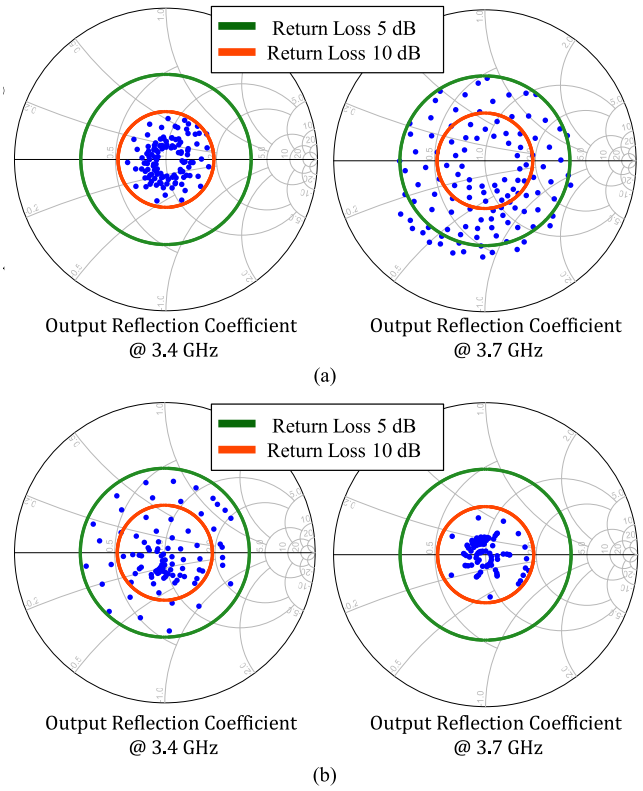

FIGURE 11. Simulated load impedance coverage (a) at the higher band when lower band for c1= 1.5 pF, cp1= 0.9 pF, c2 sweep from 0.22 pF to 0.55 pF in 0.05 pF steps, and cp2 sweeps from 0.45 pF to 2.2 pF in 20 steps, (b) at the lower band when lower band for c2= 0.2 pF, cp2= 0.6 pF, c1 sweep from 0.5 pF to 1.6 pF in 0.2 pF steps, and cp1 sweeps from 0.45 pF to 2.2 pF in 13 steps.

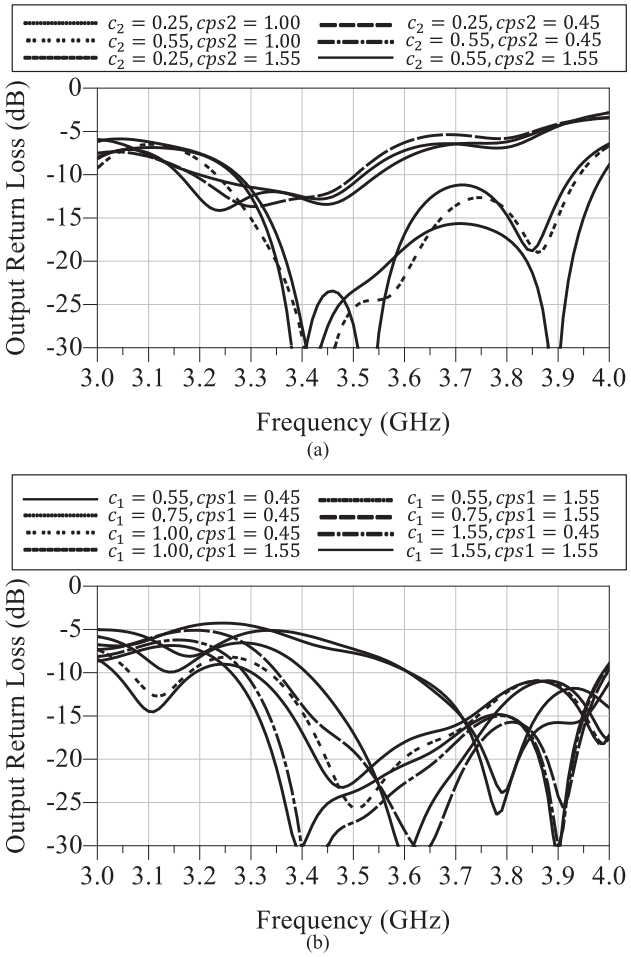

FIGURE 12. The simulated S-parameters for achieving coverage over (a) higher band and (b) lower band.

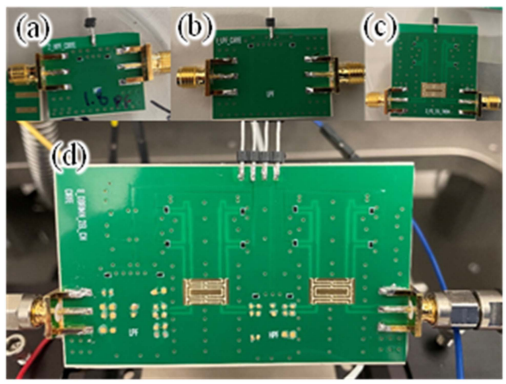

FIGURE 13. Fabricated circuits (a) Filter-1, (b) Filter-2, (c) RTPS, and (d) the proposed Db-RIMN.

For measuring the performance of the entire Db-RIMN, the two ports are calibrated to 50 Ω broadband load. Then the measured results are terminated with variable load impedances in ADS environment instead of terminating the circuit with physical load impedances. This method has the advantages of being able to evaluate the insertion loss of the circuit by modifying the impedance of the output port. four independent bias voltages are applied. The bias voltage range for the filters is similar to the individual filter measurements. For the phase shifters the voltage is between 4 V and 17 V to avoid excessive losses. A total of 110 random measurement points are collected and the coverage is depicted in Fig. 16.

The matched results in terms of output reflection coefficient and the insertion loss, for a few example loads are depicted in Fig. 17. As can be seen, different bandwidths and insertion losses are recorded at each band. The poor insertion loss performance is consistent with the sub-component measurements and is mainly due to the limited quality factor of the tuning elements and post processing of the circuit. Note that the results presented in Figs. 16 and 17 are derived by terminating the circuit in matched loads, recording the measuremnt results after aplying different bias conditions. These measuremenmt results are the terminated in Keysight ADS with variable loads. This is employed since it is impractical to fabricate tunable load impedances that change from one band to the other. Besides, this method allows studying the insertion loss.

Finally, the relationship between reflection coefficient of the load, the matched bandwidth and insertion loss are investigated in Fig. 18. To derive these trends, a handful of load impedances with similar magnitude of the reflection coefficient (i.e., with different phase). Then their bandwidths and

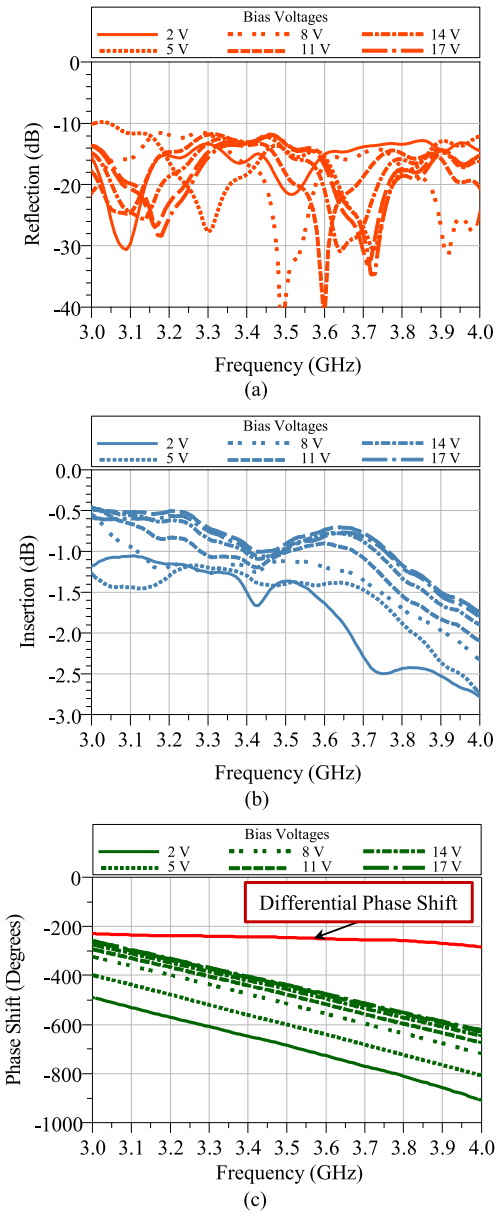

FIGURE 14. Measured results for the RTPS sub-component when biased by 2V to 17V (a) return loss, (b) insertion loss, and (c) phase shift.

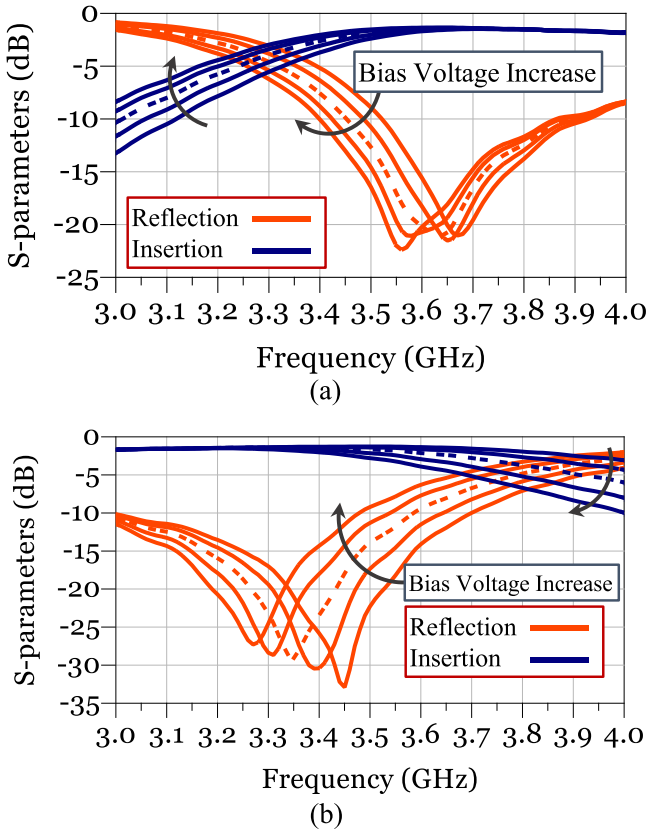

FIGURE 15. Measurement results for (a) filter-1 and (b) for filter-2.

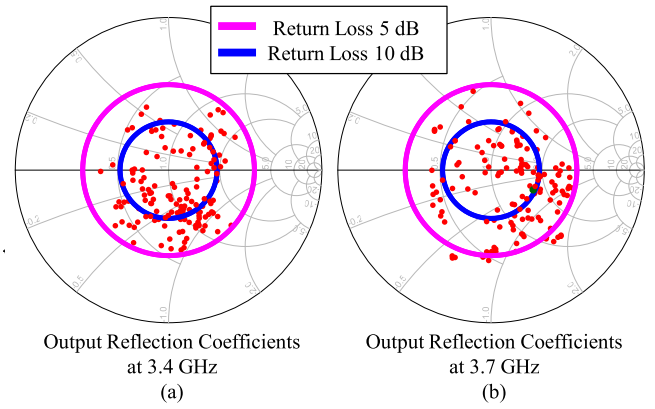

FIGURE 16. Claculated coverage achieved based on the measurements for different bias voltages (a) at 3.4 GHz and (b) at 3.7 GHz.

insertion losses are averaged separately. The results are shown for each band. The insertion loss degrades roughly by 2 and 3 dB at 3.4 GHz and 3.7 GHz, respectively. Moreover, the bandwidth is reduced by a factor of 2 and 3 at 3.4 GHz and 3.7 GHz, respectively. Accordingly, loads with worse reflection coefficients tend to have narrower bandwidth and worse insertion loss.

A comparison between the proposed Db-RIMN and published studies are presented in Table 2. As opposed to the previous reconfigurable publications that could only provide matching at one of the bands at a time, the proposed tunable design is capable of concurrent matching at both frequencies and for variable loads. Moreover, its coverage is not limited due to the use of TL segments, or switches, and its coverage is only limited by the limitations of the tuning elements. Moreover, the proposed Db-RIMN can achieve the smallest frequency ratios among the previous works.

V. CONCLUSION

A novel design theory and realization technique for designing Dual-band Reconfigurable Impedance Matching Networks (Db-RIMNs) was presented. The sub-component choices were addressed. The impacts of imperfections of the tuning elements and circuit choices were also investigated. The

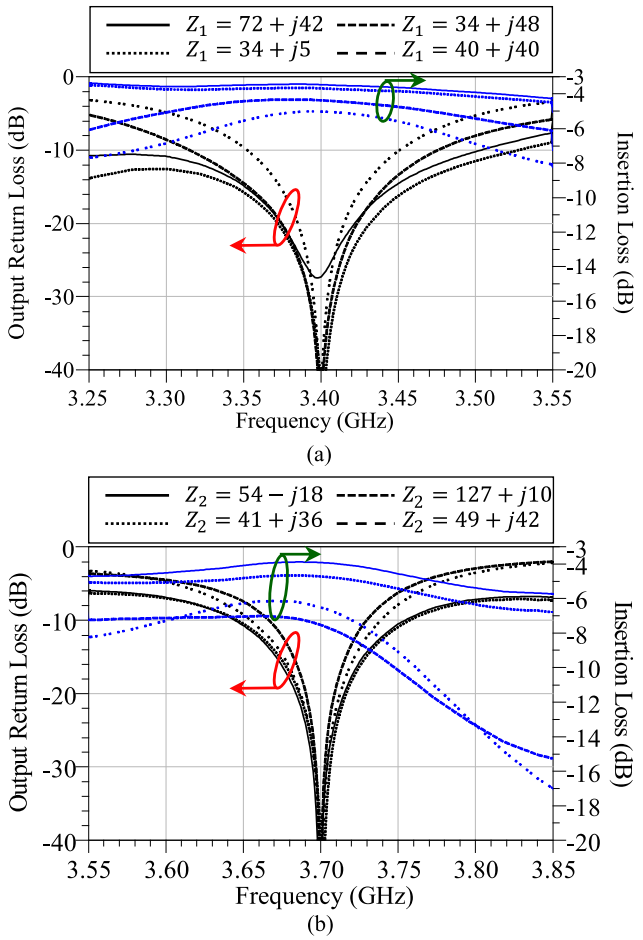

FIGURE 17. Derived S-parameters for a selection of load impedances based on the measurements for different bias voltages (a) over lower band and (b) over the higher band.

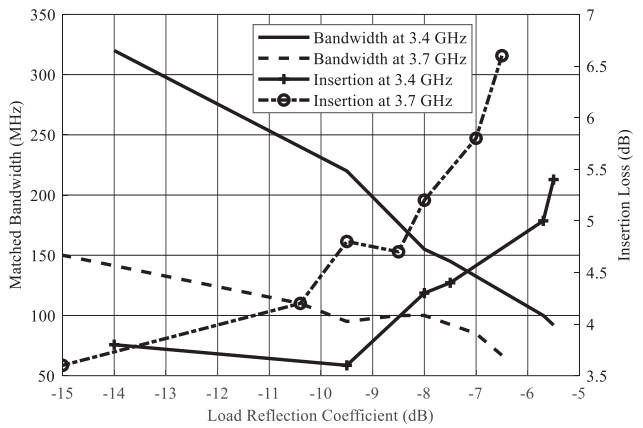

FIGURE 18. Average bandwidth and insertion loss based on the magnitude of the reflection coefficient of the load.

performance of the proposed circuit can be significantly improved at higher frequencies, where integrated solutions provide high quality factor tuning elements. To the knowledge of the authors, this work is the only theoretical and experimentally proven method for designing Db-RIMNs. A wide array of applications is anticipated for the proposed Db-RIMN, which may include concurrent PAs, multiband transceivers, millimeter wave transceiver, and high-power transmitters.

TABLE 1. Dimensions of the TL Segments for the BPFs

Parameters	Filter 1 Dimensions (mm)	Filter 2 Dimensions (mm)
Lm	11.55 (90° @ 2.9 GHz)	7.62 (90° @ 4.4 GHz)
Lo	7.94	2.85
Ls	8.00	9.64
Wm	0.38	0.49
Wo	0.35	0.46
Ws	0.31	0.48
gm	0.16	0.13
go	0.3	0.17
gs	0.28	0.12

TABLE 2. Comparison Between Dual-Band Reconfigurable Matching Networks

Ref.	[4]	[5]	[6]	[7]	This Work
Solution	Bridged-T coil (not tunable)	Switched cap.	Switched TLTs	Semi-conductor switched cap.	Tunable filters & phase shifters
Freq. (GHz)	2.4/5.5	LTE-M bands 3&4/12-20	26.5/37	2.4/5.5	3.4/3.7
Freq. Ratio	2.3	2.89-2.18	1.39	2.29	1.09
Tech.	IPD (on-chip)	PCB Mech. switched	28-nm CMOS	40-nm CMOS	PCB and BSTs
Coverage limitation	Mag. coupling coefficient, 20-120Ω TLs	Cap. res., Q-factor	Scalability number of bands, Fixed load	Scalability number of bands, Fixed load	Tunning element range Quality factor
BW (%)	18/16	3.7/4	12/09	33/21	>3/>2
Tunability	No	Switched band desc. freqs.	Switched band	Switched band	Tunablity over bands, Variable load impedance
Size mm x mm	1.5 x 1.8,	40 x 30	0.66 x 0.25	1.54 x 0.54	77 x 45
Design Complexity	High	Low	High	High	Low

APPENDIX

For a maximally flat LPF with 3dB insertion loss at f_{cL}, the power loss ratio is

$$P_{LR} = 1 + \left(\frac{f}{f_{cL}}\right)^{2N}, \tag{9}$$

$$|\Gamma|^2 = \frac{f^{2N}}{f_c^{2N} + f^{2N}}, \tag{10}$$

$$f_{cL}^{2N} = \frac{f_{2L}^{2N}}{|\Gamma_{l2min}|^2}\left(1 - |\Gamma_{l2\min}|^2\right) \tag{11}$$

and,

$$f_{cL}^{2N} = \frac{f_{1U}^{2N}}{\left|\Gamma_{f1}\right|^2}\left(1 - \left|\Gamma_{f1}\right|^2\right). \tag{12}$$

Equating (11) and (12) and using logarithms to solve the equation, one can write

$$N = \frac{\log\left(\frac{1-\left|\Gamma_{f1}\right|^2}{1-|\Gamma_{l2\min}|^2}\right)}{2} + \log\left(\frac{|\Gamma_{l2\min}|}{|\Gamma_{f1}|}\right)}{\log\left(\frac{f_{2L}}{f_{1U}}\right)}. \tag{13}$$

To determine the tuning range for the filter, one can write

$$f_{cU}^{2N} = \frac{f_{2U}^{2N}}{|\Gamma_{l2\max}|^2}\left(1 - |\Gamma_{l2\max}|^2\right). \tag{14}$$

Dividing (12) by (14) and using logarithms to solve the equation, one can write

$$\log\left(\frac{f_{cL}}{f_{cU}}\right) = \log\left(\frac{f_{2L}}{f_{2U}}\right) + \frac{\log\left(\frac{|\Gamma_{l2\max}|}{|\Gamma_{l2\min}|}\right)}{N} + \frac{\log\left(\frac{1-|\Gamma_{l2\min}|^2}{1-|\Gamma_{l2\max}|^2}\right)}{2N}. \tag{15}$$

If $f_{2L} = f_{2U}$ (i.e., higher band is a single frequency), then (15) simplifies to

$$\log\left(\frac{f_{cL}}{f_{cU}}\right) = \frac{\log\left(\frac{|\Gamma_{l2\max}|}{|\Gamma_{l2\min}|}\right)}{N} + \frac{\log\left(\frac{1-|\Gamma_{l2\min}|^2}{1-|\Gamma_{l2\max}|^2}\right)}{2N}. \tag{16}$$

Moreover, if the magnitude of the reflection coefficient of the load does not change (i.e., load impedance is located on a constant VSWR circle on the Smith chart), then (16) further simplifies to

$$\log\left(\frac{f_{cL}}{f_{cU}}\right) = \log\left(\frac{f_{2L}}{f_{2U}}\right). \tag{17}$$

Similar expressions can be derived for a HPF used in a SBITE that has a matching state over the lower band and passing state over the higher band. In this case, the return loss is intended to cover the values between $|\Gamma_{l1min}|$ and $|\Gamma_{l1max}|$ over the lower band and be better than Γ_{f2} over the higher band. The minimum order of the HPF can be written as

$$N = \frac{\log\left(\frac{1-\left|\Gamma_{f2}\right|^2}{1-|\Gamma_{l1min}|^2}\right)}{2} + \log\left(\frac{|\Gamma_{l1min}|}{|\Gamma_{f2}|}\right)}{\log\left(\frac{f_{2L}}{f_{1U}}\right)}, \tag{18}$$

which follows the same trajectory as the LPF, which is shown in Fig. 4. The tuning range can be written as

$$\log\left(\frac{f_{cL}}{f_{cU}}\right) = \log\left(\frac{f_{1L}}{f_{1U}}\right) + \frac{\log\left(\frac{|\Gamma_{l1max}|}{|\Gamma_{l1min}|}\right)}{N} + \frac{\log\left(\frac{1-|\Gamma_{l1min}|^2}{1-|\Gamma_{l1max}|^2}\right)}{2N}. \tag{19}$$

REFERENCES

[1] Y. Zhang, Y. Wu, W. Wang, Y. Yang, and L. Ma, "Novel multifunctional dual-band coupled-line coupler with reuse of low-frequency trans-directional and high-frequency contra-directional functions," *IEEE Trans. Circuits Syst. II, Exp. Briefs*, vol. 68, no. 6, pp. 1917–1921, Jun. 2021, doi: 10.1109/TCSII.2020.3042503.

[2] M. H. Maktoomi, D. Banerjee, and M. S. Hashmi, "An enhanced frequency-ratio coupled-line dual-frequency Wilkinson power divider," *IEEE Trans. Circuits Syst. II, Exp. Briefs*, vol. 65, no. 7, pp. 888–892, Jul. 2018, doi: 10.1109/TCSII.2017.2749407.

[3] M. A. Maktoomi, M. Akbarpour, M. S. Hashmi, and F. M. Ghannouchi, "On the dual-frequency impedance/admittance characteristic of multi-section commensurate transmission line," *IEEE Trans. Circuits Syst. II, Exp. Briefs*, vol. 64, no. 6, pp. 665–669, Jun. 2017, doi: 10.1109/TCSII.2016.2604425.

[4] Y.-S. Lin and C.-H. Wei, "A novel miniature dual-band impedance matching network for frequency-dependent complex impedances," *IEEE Trans. Microw. Theory Techn.*, vol. 68, no. 10, pp. 4314–4326, Oct. 2020, doi: 10.1109/TMTT.2020.3016328.

[5] H. Y. Amin, J. Chen, M. Berg, and A. Parssinen, "Tunable front-end design with a dual-band antenna for small cellular devices," in *Proc. IEEE 13th Eur. Conf. Antennas Propag.*, 2019, pp. 1–5.

[6] J. Lee, J.-S. Paek, and S. Hong, "Millimeter-wave frequency reconfigurable dual-band CMOS power amplifier for 5G communication radios," *IEEE Trans. Microw. Theory Techn.*, vol. 70, no. 1, pp. 801–812, Jan. 2022, doi: 10.1109/TMTT.2021.3122533.

[7] B. Liu, X. Quan, C. C. Boon, D. Khanna, P. Choi, and X. Yi, "Reconfigurable 2.4-/5-GHz dual-band transmitter front-end supporting 1024-QAM for WLAN 802.11ax application in 40-nm CMOS," *IEEE Trans. Microw. Theory Techn.*, vol. 68, no. 9, pp. 4018–4030, Sep. 2020, doi: 10.1109/TMTT.2020.2990460.

[8] F. Yazdani and R. R. Mansour, "Realization of dual-band matching networks using cascaded filters," in *Proc. IEEE 50th Eur. Microw. Conf.*, 2020, pp. 727–730.

[9] D. M. Pozar, *Microwave Engineering*, 4th ed. Hoboken, NJ, USA: Wiley, 2012.

[10] H. Jia and R. R. Mansour, "An efficient technique for tuning and design of filters and diplexers," *IEEE Trans. Microw. Theory Techn.*, vol. 68, no. 7, pp. 2610–2624, Jul. 2020, doi: 10.1109/TMTT.2020.2984740.

[11] Y.-P. Lyu, L. Zhu, and C.-H. Cheng, "Dual-band differential phase shifter using phase-slope alignment on coupled resonators," *IEEE Microw. Wireless Compon. Lett.*, vol. 28, no. 12, pp. 1092–1094, Dec. 2018, doi: 10.1109/LMWC.2018.2875997.

[12] Q. Dong, Y. Wu, W. Chen, Y. Yang, and W. Wang, "Single-layer dual-band bandwidth-enhanced filtering phase shifter with two different predetermined phase-shifting values," *IEEE Trans. Circuits Syst. II, Exp. Briefs*, vol. 68, no. 1, pp. 236–240, Jan. 2021, doi: 10.1109/TCSII.2020.3008532.

[13] X. Tang and K. Mouthaan, "Dual-band class III loaded-line phase shifters," in *Proc. IEEE Asia-Pacific Microw. Conf.*, 2010, pp. 1731–1734.

[14] Y. Xiong, X. Zeng, and J. Li, "A tunable concurrent dual-band phase shifter MMIC for beam steering applications," *IEEE Trans. Circuits Syst. II, Exp. Briefs*, vol. 67, no. 11, pp. 2412–2416, Nov. 2020, doi: 10.1109/tcsii.2019.2963719.

[15] T. Singh, N. K. Khaira, and R. R. Mansour, "Thermally actuated SOI RF MEMS-based fully integrated passive reflective-type analog phase shifter for mmWave applications," *IEEE Trans. Microw. Theory Techn.*, vol. 69, no. 1, pp. 119–131, Jan. 2021, doi: 10.1109/tmtt.2020.3018141.

[16] P. Gu and D. Zhao, "Geometric analysis and systematic design of a reflective-type phase shifter with full 360° phase shift range and minimal loss variation," *IEEE Trans. Microw. Theory Techn.*, vol. 67, no. 10, pp. 4156–4166, Oct. 2019, doi: 10.1109/TMTT.2019.2933213.

[17] T. W. Li and H. Wang, "A millimeter-wave fully integrated passive reflection-type phase shifter with transformer-based multi-resonance loads for 360° phase shifting," *IEEE Trans. Circuits Syst. I, Reg. Papers*, vol. 65, no. 4, pp. 1406–1419, Apr. 2018, doi: 10.1109/TCSI.2017.2748078.

[18] R. Mongia, I. Bahl, and P. Bhartia, *RF and Microwave Coupled-Line Circuits*, Norwood, MA: Artech House, 2007.